

# Extrinsic Curvature Embedding Diagrams

J. L. Lu <sup>(1)</sup> and W.-M. Suen <sup>(2,3)</sup>

<sup>(1)</sup> *Physics Department, Hunan Normal University, Hunan, P. R. China*

<sup>(2)</sup> *Department of Physics, Washington University, One Brookings Drive, St. Louis, MO 63130,  
USA*

<sup>(3)</sup> *Department of Physics, Chinese University of Hong Kong, Shatin, Hong Kong*

(To be submitted to Physical Review D, February 7, 2008)

## Abstract

Embedding diagrams have been used extensively to visualize the properties of curved space in Relativity. We introduce a new kind of embedding diagram based on the *extrinsic* curvature (instead of the intrinsic curvature). Such an extrinsic curvature embedding diagram, when used together with the usual kind of intrinsic curvature embedding diagram, carries the information of how a surface is *embedded* in the higher dimensional curved space. Simple examples are given to illustrate the idea.

arXiv:gr-qc/0301012v1 5 Jan 2003

## I. INTRODUCTION

Embedding diagrams have been used extensively to visualize and understand properties of hypersurfaces in curved space. They are surfaces in a fiducial flat space having the same *intrinsic* curvature as the hypersurface being studied. In this paper we call the former a “model surface” and the latter a “physical surface”. A familiar example is the “wormhole” construction as the embedding diagram of the time symmetric hypersurface in the maximally extended Schwarzschild geometry [1]. Another example often used is a sheet of paper curled into a cone in the 3 dimensional flat space. With the intrinsic curvature of the conical surface being zero, the “model surface” in the embedding diagram is a flat surface.

In this paper we investigate the construction of a different kind of embedding diagrams. We examine the construction of a model surface (in a fiducial flat space) having the same *extrinsic* curvature as the physical surface. Such an *extrinsic* curvature embedding diagram describes not the geometry of the physical surface, but instead how it is *embedded* in the higher dimensional physical spacetime. (For convenient of description, in this paper we will discuss in terms of a 3 dimensional spacelike hypersurface in the 4 dimensional spacetime. The same idea applies to a surface of any dimension in a space of any higher dimensions).

It is of interest to note that such an extrinsic curvature embedding diagram carries two senses of “embedding”: (1) It is a surface “embedded” in a fiducial flat space to provide a representation of some properties of the physical surface (the meaning of embedding in the usual kind of embedding diagram based on intrinsic curvature), and (2) the diagram is also representing how the physical surface is “embedded” in the physical spacetime. The extrinsic curvature embedding carries information complimentary to the usual kind of embedding diagram showing the intrinsic curvature (which we call “intrinsic curvature embedding” in this paper). For example, in the case of the constant Schwarzschild time hypersurface in a Schwarzschild spacetime, the *extrinsic* curvature embedding is a flat surface. For the case of the curled paper, the extrinsic curvature embedding is a conical surface.

In addition to its pedagogical value (like those of intrinsic curvature embedding in pro-

viding visual understanding), such extrinsic curvature embedding may help understand the behavior of different time slicings in numerical relativity, and properties of different foliations of spacetimes. Some elementary examples are worked out in this paper as a first step in understanding extrinsic curvature embedding.

## II. INTRINSIC V.S. EXTRINSIC CURVATURE EMBEDDING

In the usual kind of embedding diagram (the intrinsic curvature embedding) one constructs a “model” surface in a fiducial flat space which has the same intrinsic geometry as the physical surface, in the sense of having the same induced metric. It should immediately be noted that in general it is impossible to match all metric components of the two surfaces [2]. For example, for a 3 dimensional (3D) surface in a 4D curved space, the induced metric  $g_{ij}$  ( $i, j = 1, 2, 3$ ) (the first fundamental form) has 6 components, each of which is function of 3 variables ( $x_1, x_2, x_3$ ). The 3D model surface in the fiducial 4D flat space (with flat metric in coordinates  $(\tilde{x}^0, \tilde{x}^1, \tilde{x}^2, \tilde{x}^3)$ ) is represented by only one function of 3 variables  $\tilde{x}^0 = \tilde{x}^0(\tilde{x}^1, \tilde{x}^2, \tilde{x}^3)$ . There are 3 more functions one can choose, which can be regarded either as making a coordinate change in the physical or model surface, or as choosing the mapping between a point  $(x_1, x_2, x_3)$  on the physical surface to a point  $(\tilde{x}^1, \tilde{x}^2, \tilde{x}^3)$  on the model surface. Altogether, there are 4 arbitrary functions (e.g.,  $\tilde{x}^0 = \tilde{x}^0(\tilde{x}^i)$ ,  $\tilde{x}^i = \tilde{x}^i(x^j)$ ,  $i, j = 1, 2, 3$ ) at our disposal. In general we cannot match all 6 components of the induced metric. Only certain components can be matched, and the embedding can only provide a representation of these components. An alternative is to construct an embedding with the model surface in a higher dimensional space [3–5].

In the case of a stationary spherical symmetric spacetime like the Schwarzschild spacetime, and when one is examining the geometry of a constant-Killing-time slice, one can choose a coordinate system (e.g., the Schwarzschild coordinate) in which there is only one non-trivial induced metric component (e.g., the radial metric component). This component can be visualized with an embedding diagram using the trivial mapping  $\tilde{x}^1 = x_1$ ,  $\tilde{x}^2 = x_2$ ,

$\tilde{x}^3 = x^3$  between the physical space and the fiducial space, with  $x^1 = r$  being the circumferential radius,  $x^2 = \theta$  and  $x^3 = \phi$ . This leads to the “wormhole” embedding diagram in textbooks and popular literature.

Next we turn to extrinsic curvature embedding diagrams. To illustrate the idea, we discussed in terms of a 3D spacelike hypersurface in a 4D spacetime. Consider a constant time hypersurface in a 4D spacetime with the metric given in the usual 3 + 1 form

$$dS^2 = -(\alpha dt)^2 + g_{ij}(dx^i + \beta^i dt)(dx^j + \beta^j dt) \quad . \quad (2.1)$$

$\alpha$  is the lapse function,  $\beta^i$  is the shift vector, and  $g_{ij}$  is the spatial 3-metric of the constant  $t$  hypersurface. The extrinsic curvature (the second fundamental form) expressed in terms of the lapse and shift function is

$$K_{ij} = \frac{1}{2\alpha} \left( \beta_{i/j} + \beta_{j/i} - \frac{\partial g_{ij}}{\partial t} \right) \quad . \quad (2.2)$$

Here “/” represents covariant derivative in the three-dimensional space.

We seek a surface  $\tilde{t} = f(\tilde{x}^i)$  with the same extrinsic curvature  $K_{ij}$  embedded in a fiducial 4D flat spacetime

$$dS^2 = -(d\tilde{t})^2 + \delta_{ij} d\tilde{x}^i d\tilde{x}^j \quad . \quad (2.3)$$

It is easy to see that the extrinsic curvature of the surface  $\tilde{t} = f(\tilde{x}^i)$  is given by

$$K_{ij} = \frac{1}{2\bar{\alpha}} \left( \bar{\beta}_{i/j} + \bar{\beta}_{j/i} \right) \quad , \quad (2.4)$$

where  $\bar{\alpha} = \sqrt{1 + \frac{\partial f}{\partial \tilde{x}^i} \frac{\partial f}{\partial \tilde{x}^j} g^{ij}}$ ,  $\bar{\beta}_i = -\frac{\partial f}{\partial \tilde{x}^i}$ , and the covariant derivative in  $\bar{\beta}_{i/j}$  is with respect to a 3-metric  $\bar{g}_{ij}$  defined by  $\bar{g}_{ij} = \delta_{ij} - \frac{\partial f}{\partial \tilde{x}^i} \frac{\partial f}{\partial \tilde{x}^j}$ .  $\bar{g}^{ij}$  is the matrix inverse of  $\bar{g}_{ij}$ .

For any given 3 hypersurface in a 4D spacetime, we have only 4 functions that we can freely specify ( $f(\tilde{x}^i)$  and the 3 spatial coordinate degrees of freedom), but there are 6  $K^{ij}$  components to be matched. In general we can only have embedding representations of 4 of the components of the extrinsic curvature unless we go to a higher dimensional space, just like in the case of intrinsic curvature embedding. This brings a set of interesting questions:

Under what conditions will a surface be fully “extrinsically-embeddable” in a fiducial flat space one dimensional higher? How many dimensions higher must a fiducial space be in order for a general surface to be extrinsically-embeddable? We hope to return to these questions in future publications.

The two kinds of embedding diagrams, intrinsic curvature embedding and extrinsic curvature embedding, are supplementary to one another and can be used together. The information contained in the usual kind of intrinsic embedding diagram is partial in the sense that different slicings of the same spacetime will give different intrinsic curvature embedding diagrams, and this information of which slicing is used (the choice of the “time” coordinate) is contained in the extrinsic curvature embedding. Similarly, the information given in the extrinsic curvature embedding is partial, in the sense that the extrinsic curvature components depend on the choice of the spatial coordinates, an information that is contained in the intrinsic curvature embedding.

With the two kinds of embedding diagram constructed together, one can read out both the induced metric components and the extrinsic curvature components. In principle, all geometric properties of the surface can then be reconstructed, including how the surface is embedded in the higher dimensional spacetime. In the following we give explicit examples of these constructions.

### III. EXAMPLES OF EXTRINSIC CURVATURE EMBEDDING DIAGRAMS

We begin with the simple case of the Schwarzschild metric in Schwarzschild coordinate,

$$dS^2 = -\left(1 - \frac{2m}{r}\right)dt^2 + \left(1 - \frac{2m}{r}\right)^{-1} dr^2 + r^2(d\theta^2 + \sin^2\theta d\phi^2) \quad . \quad (3.1)$$

Since the metric is time independent and has zero shift, from (2.2) one sees immediately that the constant  $t$  slicing has  $K^{ij} = 0$  for all  $i$  and  $j$ . The “extrinsic curvature embedding” is obtained by identifying a point  $(r, \theta, \phi)$  to a point  $(\tilde{r}, \tilde{\theta}, \tilde{\phi})$  in the fiducial flat space  $dS^2 = -d\tilde{t}^2 + d\tilde{r}^2 + \tilde{r}^2(d\tilde{\theta}^2 + \sin^2\tilde{\theta}d\tilde{\phi}^2)$  , and by requiring the extrinsic curvatures of the physical

surface (embedded in Schwarzschild spacetime) and the model surface (embedded in flat spacetime) be the same. This leads to a flat model surface in the fiducial flat space. We see that while the *intrinsic* curvature embedding of the Schwarzschild slicing is non-trivial (as given in text books and popular articles), the *extrinsic* curvature embedding is trivial. This high-lights that the constant Schwarzschild time slicing is a “natural” foliation of the Schwarzschild geometry, in the sense that these (curved) constant-Schwarzschild- $t$  surfaces are embedded in the (curved) Schwarzschild geometry in a trivial manner: same as a flat surface embedded in a flat spacetime.

It is interesting to compare this to different time slicings in Schwarzschild spacetime. Define

$$t = t' + \int \frac{\sqrt{\frac{2m}{r}}}{1 - \frac{2m}{r}} dr \quad . \quad (3.2)$$

The Schwarzschild metric (3.1) becomes

$$dS^2 = -\left(1 - \frac{2m}{r}\right) dt'^2 - 2\sqrt{\frac{2m}{r}} dt' dr + dr^2 + r^2(d\theta^2 + \sin^2\theta d\phi^2) \quad . \quad (3.3)$$

The  $t' = \text{constant}$  surfaces have flat *intrinsic* geometry, so the intrinsic curvature embedding is trivial (the model surface is a flat surface in the fiducial flat space). But the *extrinsic* curvature embedding is non-trivial; as we shall work out below. This is just the opposite situation of the constant-Schwarzschild- $t$  slice (non-trivial intrinsic embedding but trivial extrinsic embedding).

For the extrinsic curvature embedding of the constant- $t'$  “flat slicing” of metric (3.3), with the spherical symmetry, it suffices to examine the slice  $\theta = \frac{\pi}{2}$ . A constant  $t'$  slicing in metric (3.3) has extrinsic curvature

$$K_{rr} = \frac{1}{2r} \sqrt{\frac{2m}{r}} \quad , \quad (3.4)$$

$$K_{\phi\phi} = -\sqrt{2mr} \quad . \quad (3.5)$$

The extrinsic curvature embedding is given by a  $\tilde{t} = f(\tilde{r}, \tilde{\phi})$  surface embedded in a fiducial 3D Minkowski space

$$dS^2 = -d\tilde{t}^2 + d\tilde{r}^2 + \tilde{r}^2 d\tilde{\phi}^2 \quad . \quad (3.6)$$

Using (2.4), it is straightforward to find that the non-trivial extrinsic curvature components are

$$K_{\tilde{r}\tilde{r}} = -\frac{f''}{\sqrt{1-f'^2}} \quad , \quad (3.7)$$

$$K_{\tilde{\phi}\tilde{\phi}} = -\frac{\tilde{r}f'}{\sqrt{1-f'^2}} \quad , \quad (3.8)$$

where  $f' = df/d\tilde{r}$  is a function to be determined by matching the extrinsic curvature ( $K_{\tilde{r}\tilde{r}}, K_{\tilde{\phi}\tilde{\phi}}$ ) to that of the physical surface given by (3.4), (3.5).

It is immediately clear that with only one arbitrary function  $\tilde{t} = f(\tilde{r}, \tilde{\phi})$ , it would not be possible to match both of the two non-trivial extrinsic curvature components. To enable the matching, we introduce a spatial coordinate transformation *on* the  $t' = \text{constant}$  physical surface  $r = h(r')$ . As  $K_{ij}$  is a tensor on the surface, the coordinate change will change the value of  $K_{rr}$  but *not* how the surface is embedded. Due to the spherical symmetry, it suffices to rescale only the radial coordinate, keeping the angular coordinate unchanged.

Using (3.7, 3.8) and (3.4, 3.5), and identifying the fiducial flat space coordinates  $(\tilde{r}, \tilde{\phi})$  with physical space coordinate  $(r', \phi)$ , we obtain the conditions on the functions  $f(\tilde{r})$  and  $h(r' = \tilde{r})$

$$\frac{(h')^2}{2h} \sqrt{\frac{2m}{h}} = -\frac{f''}{\sqrt{1-f'^2}} \quad , \quad (3.9)$$

$$\sqrt{2mh} = \frac{\tilde{r}f'}{\sqrt{1-f'^2}} \quad , \quad (3.10)$$

where  $h' = dh/d\tilde{r}$ . The boundary conditions for the system are (i)  $f'$  tends zero at infinity, and (ii)  $h$  tends to  $\tilde{r}$  at infinity; that is, the embedding is trivial asymptotically. The two equations lead to a quadratic equation for  $f''$  with the two roots

$$f'' = -\frac{f'(1-f'^2)}{4\tilde{r}} \left( (5-f'^2) \pm \sqrt{(1-f'^2)(9-f'^2)} \right) \quad . \quad (3.11)$$

While both the “+” and the “-” sign solutions satisfy the boundary condition (i) for  $f'$ , it is easy to see that only the “-” solution leads to a  $h(\tilde{r})$  that satisfies the boundary condition

(ii) for  $h$ . Integration of the 2nd order equation associated with the “-” solution gives the extrinsic curvature embedding diagram for the spatially flat constant time slicing of the Schwarzschild spacetime as shown in Fig. 1. The height of the surface is the value of  $f$ , the horizontal plane is the  $(\tilde{r}, \phi)$  plane (recall  $\tilde{r} = r'$ ). All quantities are in unit of  $m$  (i.e.,  $m = 1$ ).

In what sense does this figure provide a “visualization” of the extrinsic curvature  $K_{ij}$  of the physical surface? The extrinsic curvature compares the normal of the surface at two neighboring points (cf. Sec. 21.5 of [1]). In Fig. 1, with the model surface embedded in a flat space, one can easily visualize (i) unit vectors normal to the surface, (ii) the parallel transport of a unit normal vector to a neighboring point, and (iii) the subtraction of the transported vector from the unit normal vector at the neighboring point, all in the usual flat space way. For example, in Fig. 1, imagine unit normals at two neighboring points  $(r, \phi)$  and  $(r, \phi + d\phi)$ . With the horn shape surface, the “tips” of the unit normal vectors are closer than their bases. When parallel transported, subtracted and projected into the  $\phi$  direction (all done in the flat space sense) this gives the value of  $K_{\phi\phi}$ . On the other hand, if we compare the normals of the neighboring points  $(r, \phi)$  and  $(r + dr, \phi)$ , the “tips” of the normal vectors are further away than their bases. This accounts for the difference in sign of  $K_{rr}$  and  $K_{\phi\phi}$  in (3.4) and (3.5). Also explicit visually is the fact that, at large  $r$ , the unit normals at neighboring points (both in the  $r$  and  $\phi$  directions) become parallel, showing that the extrinsic curvature goes to zero. (Notice that  $K_{\phi\phi}$  is not going to zero as  $d/d\phi$  is not a unit vector; rather, the extrinsic curvature contracted with the *unit* vector in the  $\phi$  direction is going to zero as  $r^{-3/2}$  in the same way as  $K_{rr}$ .) We note that  $f$  does not tend to a constant but is proportional to  $\sqrt{r}$  at large  $r$ , although  $f'$  does go to zero as implied by the boundary condition.

We note that this prescription of visualizing the covariant components of the extrinsic curvature  $K_{ij}$  is precisely the flat space version of the prescription given in Sec. 21.5 of [1]. While the directions of the normal vectors and the result of a parallel transport are not readily visualizable in the curved space construction given in [1], the use of an embedding



diagram in a fiducial flat space enables the easy visualization of normal vectors and their parallel transport— as all of them are constructed in the usual flat space sense. It is also for the easiness of visualization that we choose to work with the covariant component of the extrinsic curvature. While the contravariant components can be treated equivalently (note that we are working with spacetimes endowed with metrics), its visualization involved one-form which is less familiar (see however the visualization of forms in [1]).

Returning to the example at hand, we show in Figs. 2a and 2b the “scaling function”  $h(\tilde{r})$  v.s.  $\tilde{r}$ . We see that  $h$  is linear in  $\tilde{r}$  for large  $\tilde{r}$ , satisfying the boundary condition (ii). In Fig. 2a, we see that  $h$  is nearly linear throughout. To see that  $h$  is not exactly linear, we show in Fig. 2b that  $h' - 1$  is appreciably different from zero in the region of smaller  $r$ . This small difference from exact linearity is precisely what is needed to construct a model surface that can match both  $K_{rr}$  and  $K_{\phi\phi}$ .

We see that the embedding is perfectly regular at the horizon ( $r = 2$ ). It has a conical structure at  $\tilde{r} = 0$ , in the sense that  $f'$  is not going to zero but instead approaches 1 from below (i.e.,  $f' \sim 1 - a2\tilde{r}^2$  for small  $\tilde{r}$ ). Although the surface covers all  $\tilde{r}$  values, we note that  $h(\tilde{r})$  approaches a constant  $\sim 0.2$ , implying that the embedding diagram does *not* cover the inner-most region (from  $r = 0$  to  $r \sim 0.2m$ ) of the the circumferential radius  $r$ . Comparing this to the constant-Schwarzschild-time slicing (constant  $t$  slicing in metric (3.1)) is again interesting: The *intrinsic* curvature embedding of the constant-Schwarzschild-time slicing also does not cover the inner-region (from  $r = 0$  to  $r = 2m$ ), while the *extrinsic* curvature embedding of the constant-Schwarzschild-time slicing covers all  $r$  values just like the *intrinsic* curvature embedding of the “spatially flat” slicing.

We emphasize again that the extrinsic curvature embedding diagram Fig. 1 does *not* carry any information about the intrinsic geometry of the surface. For example, the circumference of a circle at a fixed  $\tilde{r}$  is not  $2\pi\tilde{r}$ , and the distance on the model surface is not the physical distance between the corresponding points on the physical surface (unlike the case of the intrinsic curvature embedding diagram). This extrinsic curvature embedding diagram Fig. 1 carries only the information of how the “spatially flat” slicing is embedded in the

Schwarzschild geometry, in the sense that the relations between the normal vectors of the slicing embedded in the curved Schwarzschild spacetime are the same as given by the surface shown in Fig. 1 embedded in a flat Minkowski spacetime.

One might want to obtain the physical distance between two neighboring points, say, at  $\tilde{r}$  and  $\tilde{r} + d\tilde{r}$ , in Fig. 1. This information is contained in Figs.2a and 2b, as the scaling factor  $h$  gives the relation between  $r$  and  $\tilde{r} = r'$ .

One can also give a visual representation of this information of the intrinsic geometry by plotting an *intrinsic* embedding diagram, as in Fig. 2c. For this spatially flat slicing, the *intrinsic* embedding diagram is a flat surface in a fiducial flat space. To enable this intrinsic embedding diagram Fig.2c to be used conveniently with the extrinsic embedding diagram Fig. 1., we have plotted Fig. 2c in a way different from what is usually done in plotting embedding diagrams: The labeling of the spatial coordinate in this diagram is given in  $r'$ , the same coordinate (note  $\tilde{r} = r'$ ) as used in the extrinsic embedding diagram (or more precisely, it is  $x' = r' \cos(\phi)$ , and  $y' = r' \sin(\phi)$ ). In this way, the physical distance between any two coordinate points  $r'_1$  and  $r'_2$  in the *extrinsic* curvature embedding Fig. 1 (remember  $r' = \tilde{r}$ , the coordinate used in Fig. 1) can be obtained directly by measuring the distance on the model surface between the corresponding two points  $r'_1$  and  $r'_2$  in Fig. 2c. Hence, between this pair of intrinsic and extrinsic embedding diagrams, we can obtain all necessary information about the physical surface, with both the first (metric) and second (extrinsic curvature) fundamental forms explicitly represented.

We note that in Fig. 2c, the coordinate labels are very close to equally spaced. This is a reflection of the fact that the scaling function  $h$  given in Fig. 2a is very close to being linear (but not exactly). This near-linearity of the scaling function, together with the fact the intrinsic embedding diagram is flat, tell us that in this special case, the physical distances (the physical metric) on the *extrinsic* curvature embedding surface in Fig. 1 between points are, to a good approximation, given simply by their coordinate separations in  $r'$  (while the extrinsic curvature is contained in the shape of the surface). Obviously this would not be true in general.

Next we turn to another simple example. The infalling Eddington-Finkelstein coordinate  $V$  is defined by  $V \equiv t + r^* = t + r + 2m \ln\left(\frac{r}{2m} - 1\right)$ . Let

$$\bar{t} \equiv V - r = t + 2m \ln\left(\frac{r}{2m} - 1\right) . \quad (3.12)$$

The Schwarzschild metric in the ‘‘infalling  $\bar{t}$  slicing’’ becomes

$$dS^2 = -\left(1 - \frac{2m}{r}\right) d\bar{t}^2 + \frac{4m}{r} d\bar{t} dr + \left(1 + \frac{2m}{r}\right) dr^2 + r^2(d\theta^2 + \sin^2\theta d\phi^2) . \quad (3.13)$$

Both the intrinsic and extrinsic curvature embedding diagrams of the infalling  $\bar{t}$  slicing are non-trivial. In the following we work out the extrinsic curvature embedding.

The extrinsic curvature of the ‘‘infalling slicing’’ is given by

$$K_{ij} = \begin{pmatrix} -\frac{2m}{r^2} \frac{1+\frac{m}{r}}{\sqrt{1+\frac{2m}{r}}} & 0 & 0 \\ 0 & \frac{2m}{\sqrt{1+\frac{2m}{r}}} & 0 \\ 0 & 0 & \frac{2m \sin 2\theta}{\sqrt{1+\frac{2m}{r}}} \end{pmatrix} . \quad (3.14)$$

Again with the spherical symmetry it suffice to study the slicing  $\theta = \frac{\pi}{2}$ . To construct the extrinsic embedding, we (i) introduce a coordinate scaling  $r = h(r')$ , (ii) identify the coordinate  $(r', \phi)$  with  $(\tilde{r}, \tilde{\phi})$  of (3.6), and (iii) require  $K_{r'r'} = K_{rr}$ ,  $K_{\phi\phi} = K_{\tilde{\phi}\tilde{\phi}}$ . This leads to the following equations for  $f$  and  $h$ :

$$-\frac{\tilde{r} f'}{\sqrt{1-f'^2}} = \frac{2m}{\sqrt{1+\frac{2m}{h}}} , \quad (3.15)$$

$$-\frac{f''}{\sqrt{1-f'^2}} = -\frac{2m(h')^2}{h^2} \frac{1+\frac{m}{h}}{\sqrt{1+\frac{2m}{h}}} . \quad (3.16)$$

Eliminating  $h$  leads to a quadratic equation for  $f''$ , the two roots of which give two second order equations for  $f$ . We omit the rather long expressions here. Again only one of the two equations admit a solution with the correct asymptotic behavior at large  $\tilde{r}$  ( $f'$  tends to zero and  $h$  tends to  $\tilde{r}$ ). Integrating this second order equation gives the embedding diagram shown in Fig. 3. The height of the surface represents the value of  $f$ , the horizontal plane is the  $(\tilde{r}, \phi)$  plane. All quantities are in unit of  $m$ . Fig. 4a gives the scaling function  $h(\tilde{r})$  v.s.  $\tilde{r}$ , showing that it satisfies the boundary condition at infinity. Asymptotically  $h$  tends

to  $\tilde{r}$ , while  $f \sim -2m \log(\tilde{r})$ , and  $f' \sim \frac{-2m}{r} + \frac{2m^2}{r^2}$ . Again we see that  $h$  is very close to being linear. To show that it is not exactly linear, we plot in Fig. 4b the derivative of  $h$  v.s.  $r'$ . For  $r' < 2m$ , the derivative is considerably less than 1.

As one may expect, the embedding is regular at the horizon, but has a conical structure at  $\tilde{r} = 0$ , same as the “spatially flat slicing” case above. For small  $\tilde{r}$ ,  $f'$  tends to  $-1$  (from above), while  $h$  tends to a constant  $\sim 1.2m$ . This implies that the inner most region of the circumferential radius  $r$  (from 0 to  $1.2m$ ) is not covered in the embedding diagram, again similar to the “spatially flat slicing” extrinsic curvature embedding studied above.

We see that while the model surface in the “spatially flat slicing” embedding diagram Fig. 1 dips down for small  $\tilde{r}$ , the model surface in the “infalling slicing” embedding diagram Fig. 3 spikes up. This is expected as the signs of the extrinsic curvature components ( $K_{rr}, K_{\phi\phi}$ ) are opposite of one another for the two slicings. We can easily see in Figs. 1 and 3, that in one case “the tips of the normal are closer than their base” or vice versa. Such visual inspection is possible as the model surfaces are now embedded in flat spaces, enabling the use of flat space measure of distances, and normal vectors.

Again, one might want to visualize the physical distance between two neighboring points in Fig. 3. This can be done by plotting the corresponding *intrinsic* embedding diagram in the  $r'$  coordinate, as is given in Fig. 4c. The physical distance between any two coordinate points  $r'_1$  and  $r'_2$  can be measured by their distance on this *intrinsic* embedding surface, in the flat space way. Due to the near linearity of the scaling function  $h$ , we see that the coordinate labels are again very close to equally spaced. However, in this case, unlike the spatially flat slicing above, the physical distance between the same coordinate distance  $dr'$  is larger for smaller  $r'$ , as we can see from the curving of the intrinsic embedding surface. Between this pair of intrinsic and extrinsic embedding diagrams, we can again visualize all information of the physical surface.

## IV. SUMMARY AND DISCUSSIONS

In this paper we propose a new type of embedding diagram, i.e., the “extrinsic curvature embedding diagram” based on the 2nd fundamental form of a surface. It shows how a surface is embedded in a higher dimensional curved space. It carries information complimentary to the usual kind of “intrinsic curvature embedding diagram” based on the 1st fundamental form of the surface. We illustrate the idea with 3 different slicings of the Schwarzschild spacetime, namely the constant Schwarzschild  $t$  slicing (Eq. (3.1)), the “spatially flat” slicing (Eq. (3.3)) and the “infalling” slicing (Eq. (3.13)). The intrinsic and extrinsic curvature embeddings of the different slicings are discussed, making interesting comparisons.

The intrinsic curvature embedding diagram depends on the choice of the “time” slice (in the 3+1 language of this paper), which is a piece of information carried in the extrinsic curvature. On the other hand, the extrinsic curvature embedding diagram constructed out of the extrinsic curvature components depends on the choice of the “spatial” coordinates, which is a piece of information carried in the intrinsic curvature embedding diagram. With the two kinds of embedding diagram constructed together, all geometric properties of the surface can then be reconstructed, including how the surface is embedded in the higher dimensional spacetime.

Why do we study embedding diagrams? One can ask this questions for both the intrinsic and extrinsic embedding constructions. It is clear that embedding construction has pedagogical value, e.g., the wormhole diagram of the Schwarzschild geometry appears in many textbooks introducing the ideas of curved spacetimes. The usual embedding diagrams shown are those based on the intrinsic curvature. Here we introduce a complimentary kind of embedding diagrams which is needed to give the full information of the surface in the curved spacetime. Beyond their pedagogical value, we would like to point out that embedding diagram could be useful in numerical relativity. Indeed the authors were led to the idea of extrinsic curvature embedding in trying to find a suitable foliation (to choose the lapse function) in the numerical construction of a black hole spacetime. In the standard

3+1 formulation of numerical relativity, the spatial metric  $g_{ij}$  and the extrinsic curvature  $k_{ij}$  are used in parallel as the fundamental variables in describing a particular time slice. One chooses a lapse function to march forward in time. A suitable choice is crucial to make both the  $g_{ij}$  and  $k_{ij}$  regular, smooth and evolving in a stable manner throughout the spacetime covered by the numerical construction. Whether a choice is suitable depends on the properties of the slicing and hence has to be dynamical in nature. This is a problem not fully resolved even in the construction of a simple Schwarzschild spacetime. Embedding diagrams let us see the pathology of the time slicing clearly and hence could help in the picking of a suitable lapse function. For example, in the constant Schwarzschild time slicing (Eq.(3.1)), the intrinsic curvature embedding dips down to infinity at  $r = 2m$  and cannot cover the region inside (the extrinsic curvature embedding is flat and nice for all  $r$ ). In the time slicing of Eq. (3.3), the intrinsic curvature embedding is flat and nice for all  $r$ , but the extrinsic curvature embedding has a conical singularity near  $r = 0.2m$  and cannot cover the region inside, as shown in Sec. 3 of this paper. For the use of embedding diagrams in numerical relativity, and in particular in looking at the stability of numerical constructions with different choices of time slicing, one would need to investigate the two kinds of embedding diagrams in dynamical spacetimes. We are working on simple cases of this presently.

## V. ACKNOWLEDGMENT

We thank Malcolm Tobias for help in preparing the figures. This work is supported in part by US NSF grant Phy 9979985.

## REFERENCES

- [1] C. W. Misner, K. S. Thorne and J. A. Wheeler, **Gravitation**, (W. H. Freeman, San. Francisco, 1973).
- [2] E. Kasner, Am. J. Math., **43**, 126, (1921).
- [3] C. Fronsdal, Phys. Rev., **116**, 778, (1959).
- [4] C. J. S. Clarke, Proc. Roy. Soc. London A, **314**, 417, (1970).
- [5] E. Kasner, Am. J. Math., **43**, 130, (1921).

## FIGURES

FIG. 1. Embedding diagram for the “spatially flat slicing” of the Schwarzschild spacetime (line element (3.3)). The function  $f$  given by (3.11) is plotted on the  $\theta = \pi/2$  plane.  $df/d\tilde{r}$  tends to 1 at the origin ( $\tilde{r}$  tends to 0), where the embedding has a conical structure. All quantities are in unit of  $m$ .

Fig. 2a. Scaling factor  $h$  defined by (3.9, 3.10) for the “spatially flat slicing” of the Schwarzschild spacetime (line element (3.3)).  $h$  tends to  $\tilde{r}$  at infinity and is basically linear through out. It tends to a non-zero constant  $\sim 0.2m$  as  $\tilde{r}$  approaches zero.

Fig. 2b. Derivative of  $h$  with respect to  $\tilde{r}$  is plotted in the close zone, showing that it is not exactly linear. This slight deviation from exact nonlinearity is needed to enable both  $k_{rr}$  and  $k_{\phi\phi}$  be matched.

Fig. 2c. The *intrinsic* curvature embedding diagram (corresponding to the *extrinsic* curvature embedding diagram in Fig.1) is plotted in  $r' = \tilde{r}$ , the same coordinate as used in Fig. 1 (or more precisely, it is  $x' = r'\cos(\phi)$ , and  $y' = r'\sin(\phi)$ ). The physical distance between any two coordinate points  $r'_1$  and  $r'_2$  in the *extrinsic* curvature embedding Fig. 1 can be obtained directly by measuring the distance in the flat space sense between the corresponding two points  $r'_1$  and  $r'_2$  on the model surface in Fig. 2c. Between Fig. 1 and 2c, we can obtain all necessary information about the physical surface, with both the first (metric) and second (extrinsic curvature) fundamental forms explicitly represented.

Fig. 3. Embedding diagram for the “infalling slicing” of the Schwarzschild spacetime (line element (3.13)). The function  $f$  defined by (3.15, 3.16) is plotted on the  $\theta = \pi/2$  plane.  $df/d\tilde{r}$  tends to 1 at the origin ( $\tilde{r}$  tends to 0), where the embedding has a conical singularity. All quantities are in unit of  $m$ .

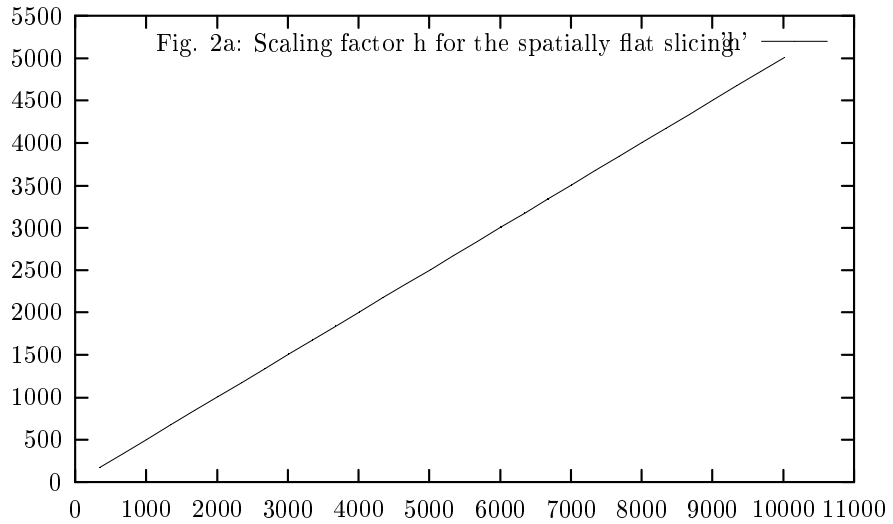
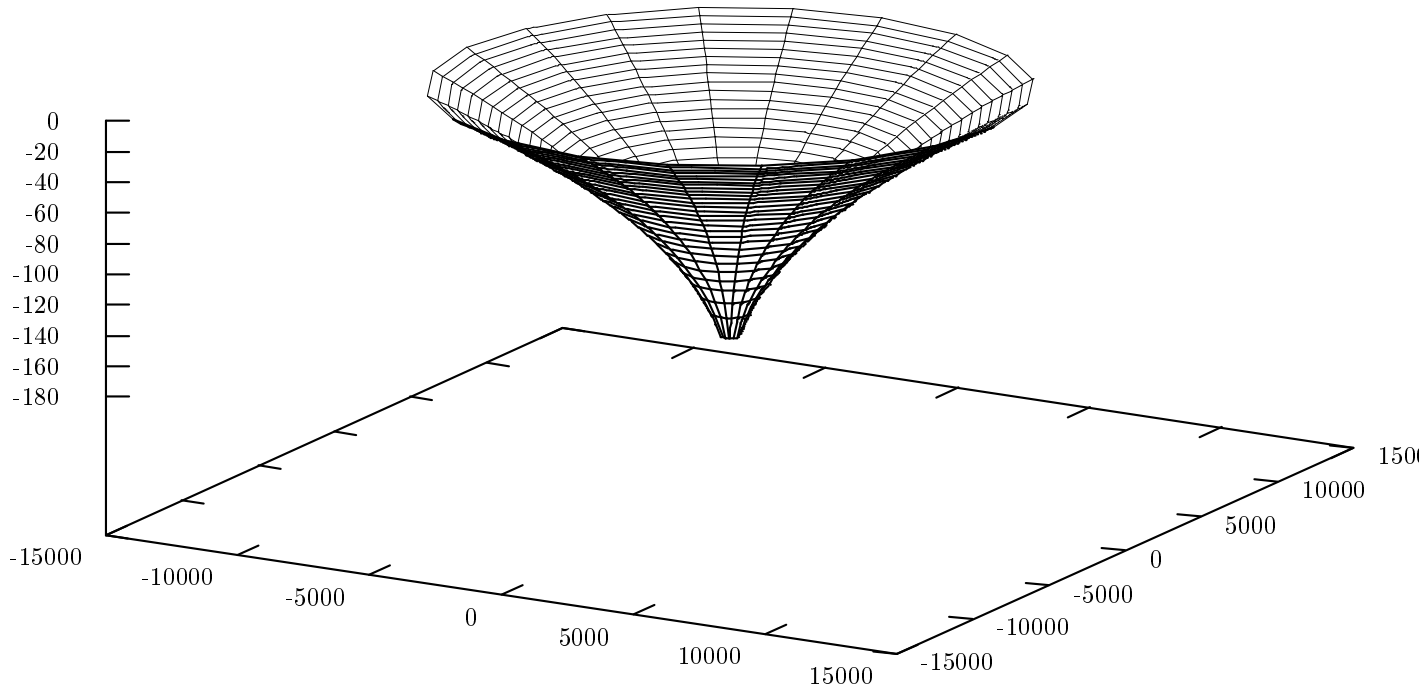
Fig. 4a. Scaling factor  $h$  defined by (3.15, 3.16) for the “spatially flat slicing” of the Schwarzschild spacetime (line element (3.13)).  $h$  tends to  $\tilde{r}$  at infinity and is nearly linear through out. It tends to a non-zero constant  $\sim 1.2m$  as  $\tilde{r}$  approaches zero.



Fig. 4b. Derivative of  $h$  with respect to  $\tilde{r}$  is plotted in the close zone for the infalling slicing, showing that it is not exactly linear.

Fig. 4c. The *intrinsic* curvature embedding diagram for the infalling slicing, corresponding to the *extrinsic* curvature embedding diagram in Fig.3, is plotted in  $r' = \tilde{r}$ , the same coordinate as used in Fig. 3. Due to the linearity of  $h$  in Fig. 4a, the coordinate labels are nearly equally spaced. The physical distance between any two coordinate points  $r'_1$  and  $r'_2$  in the *extrinsic* curvature embedding Fig. 3 can be obtained directly by measuring the distance in the flat space sense on the model surface Fig. 4c between the corresponding two coordinate points  $r'_1$  and  $r'_2$ . We see that the same coordinate separation corresponds to a large physical distance in the near zone.

Fig. 1: Embedding diagram for the spatially flat slicing



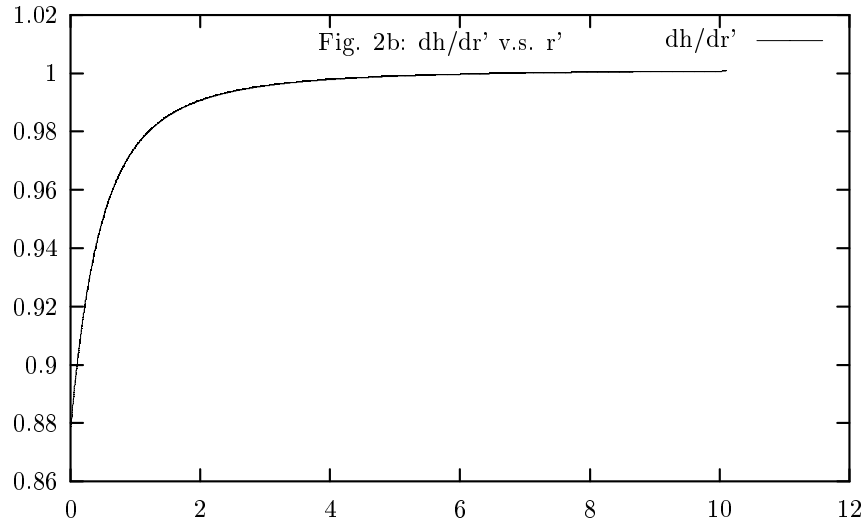


Fig. 2c: Intrinsic embedding diagram for the spatially flat slicing in the transformed  $r'$  coordinate

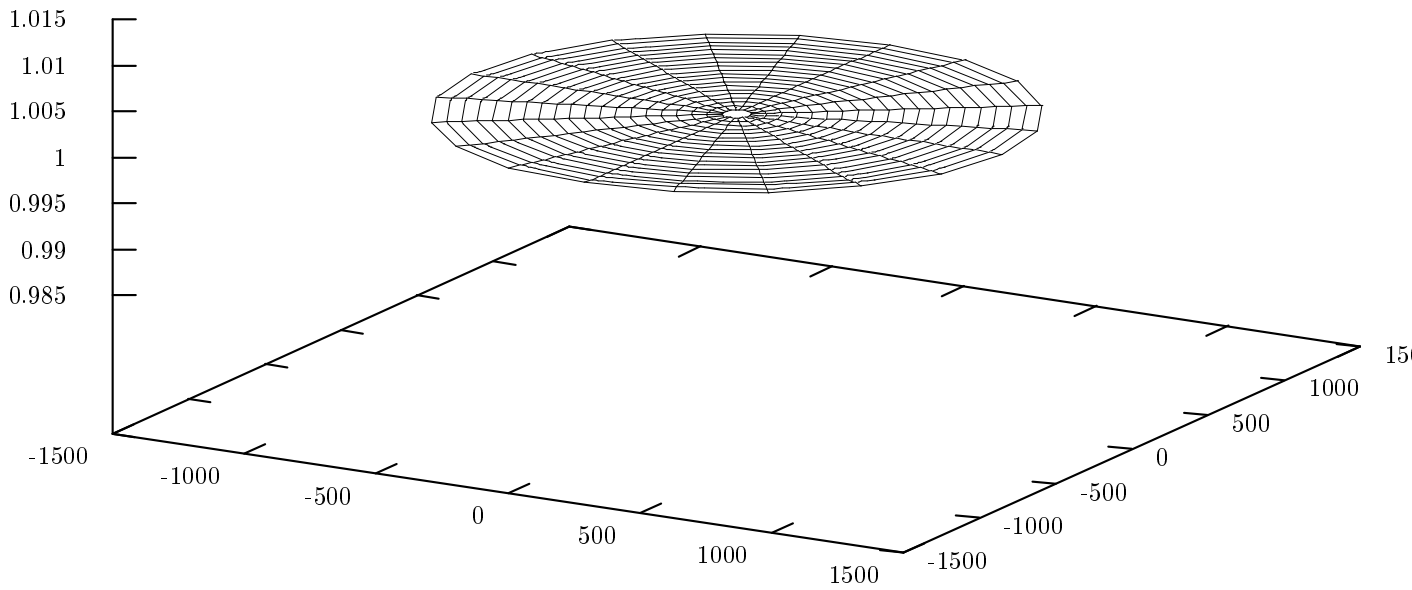


Fig. 3: Embedding diagram for infalling slicing

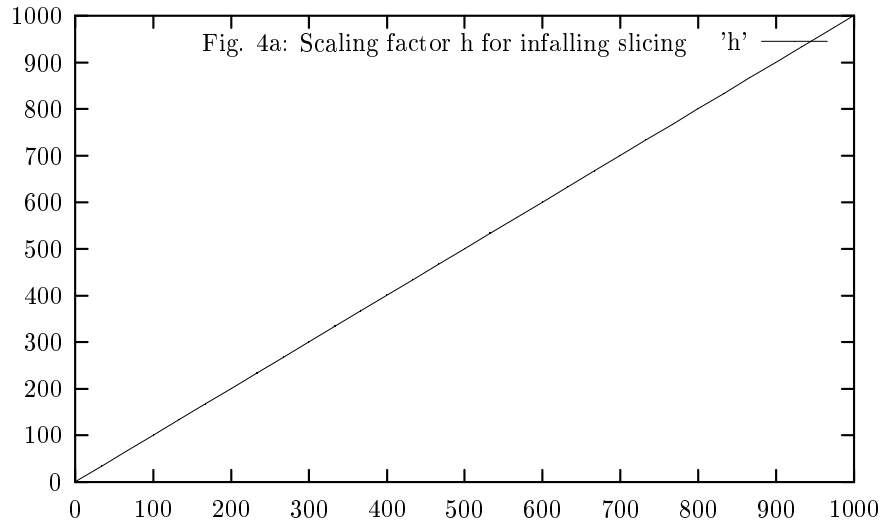
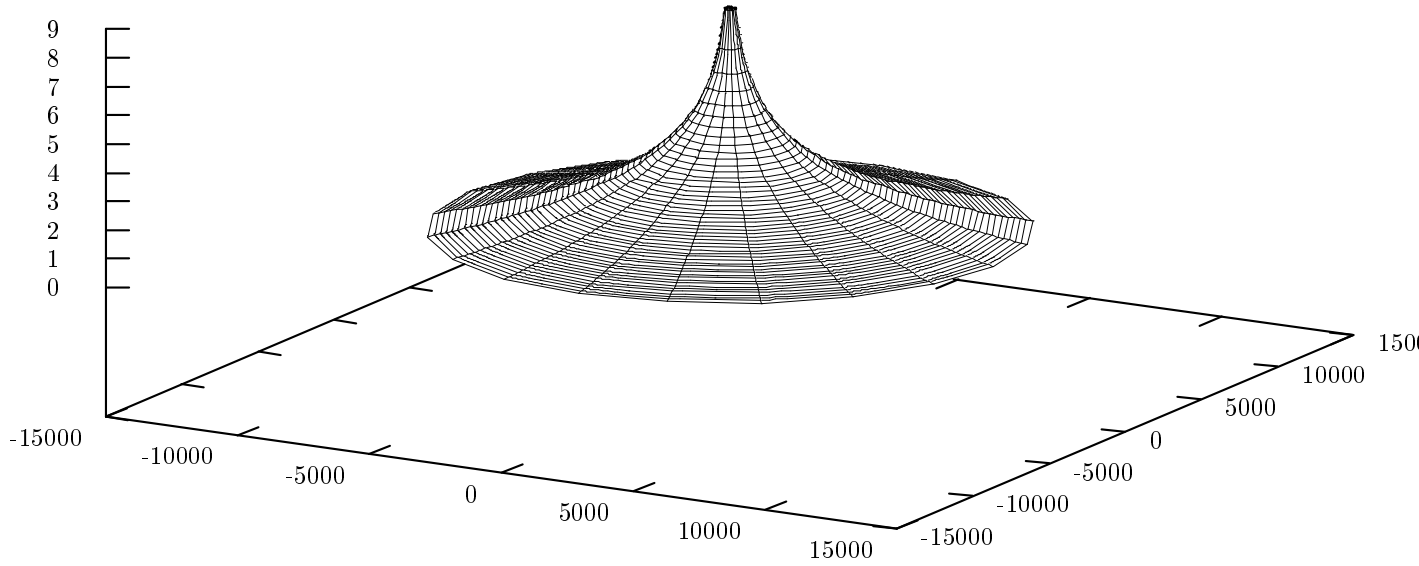


Fig. 4b:  $dh/dr'$  v.s.  $r'$

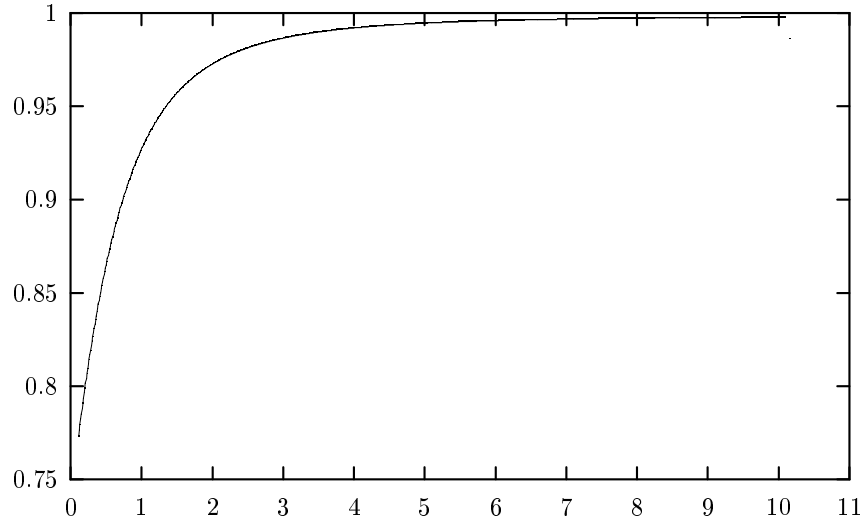


Fig. 4c: Intrinsic embedding diagram for the “infalling slicing” in the transformed  $r'$  coordinate

